Multiscale model of miscible polymer blends in porous media: From flow fields to concentration fluctuations

Gavin A. Buxton and Nigel Clarke
Department of Chemistry, University of Durham, Durham, DH1 3LE, United Kingdom
(Received 26 May 2006; published 18 October 2006)

We have developed a multiscale approach for simulating the concentration fluctuations in a miscible blend subject to complex flow dynamics. We first simulate the hydrodynamics of a fluid as it flows through porous media. In particular, we monitor the velocity gradients as a function of time for a fluid "particle" as it follows a tortuous path through the system. Next, we evolve the structure factor of the spatial concentration fluctuations subject to this flow environment. The velocity gradients experienced by this fluid particle can result in elongation and rotation of the concentration fluctuations. In this manner, we couple the macroscopic flow fields in porous media with the microscopic concentration fluctuations in the polymer blend. We find a close correlation between the tortuous pathways, the velocity gradients in the fluid, and the perturbance of the structure factor from it quiescent state. Furthermore, we find that the concentrations tend to elongate towards the flow direction or at an acute angle with the flow direction.

DOI: 10.1103/PhysRevE.74.041807 PACS number(s): 83.80.Tc, 47.56.+r

I. INTRODUCTION

Most commercial plastics are formed from the blending of two or more different polymer species [1]. In this manner materials scientists can create polymer blends which exhibit desirable characteristics associated with each of the individual polymeric constituents. For example, ductile and brittle polymers are often blended together to form a composite which possesses both acceptable strength and toughness [1,2]. The properties of the final product can depend heavily upon the processing history and, therefore, it is beneficial to understand both the thermodynamics and dynamics of molten polymer blends during industrial processing. It should be noted, however, that most commercial polymers are immiscible. The following analysis, therefore, is applicable to a minority of miscible polymer blends and polymer blends within the one-phase region.

It is well known that blends processed under simple shear often exhibit large shifts in the phase-separation temperature and, most commonly, shear-induced mixing [3,4]. The effects of shear on the thermodynamics of a polymer blend in the one-phase region can be probed by considering the concentration fluctuations [5]. In particular, a measure of the effective χ parameter can be obtained from the spatial scale of the concentration fluctuations which arise due to thermal noise in the system [6]. What is less well known is how flow patterns, more complicated than simple shear flow, can affect the spatial fluctuations in polymer concentrations and, hence, the thermodynamics of the blend. It is the purpose of this study to investigate concentration fluctuations in a miscible polymer blend *as it flows* through a tortuous porous media.

Flow in porous media is of technological importance to a wide range of scientific disciplines, including petroleum engineering, geophysics and biology [7]. However, there is also a strong academic motivation for studying fluid flow through porous media. Flow in this geometry provides an excellent opportunity for studying the behavior of fluids subject to complex flow dynamics. The complex microstructure of porous media, and the converging and diverging fluid channels, can enable us to probe the effects of extensional and shear flow on the thermodynamics of polymer blends.

We present a multiscale approach for capturing the dynamics of concentration fluctuations in a polymer blend as it flows through porous media. We first simulate the hydrodynamics of the fluid flow through the porous media and capture the flow profile. Given this flow profile we can follow a fluid "element" as it travels along a streamline through the porous media. We use the time-dependent environment that this fluid element experiences as the input to a model of the evolution of the concentration fluctuations in the polymer blend. In other words, as the fluid element traverses the porous media it experiences variations in extensional and shear flow which elongate and rotate the concentration fluctuations. By combining a model of the macroscopic hydrodynamics with a model of the nanoscale concentration fluctuations we can capture the multiscale physics of this system and correlate the complexity of the flow field to the thermodynamics of the polymer blend.

In the following section we detail the methodology for our multiscale model and describe both the lattice Boltzmann (LB) model used to capture the flow profiles and the Cahn-Hilliard model used to capture the evolution of the concentration fluctuations. The third section presents results and discussions, while we summarize our study and draw relevant conclusions in the final section.

II. METHODOLOGY

A. Lattice Boltzmann model

In this study we assume that the polymer blend can be adequately described as a simple Newtonian fluid under the limited hydrodynamic conditions considered here. In other words, to ensure that the flow field is Newtonian we assume a relatively small relaxation time of 0.001 for the polymer fluid and limit the velocity field (and, hence, shear rates) to small values. This assumption is unlikely to be valid for most commercial polymer blends subject to industrial processing.

However, we believe the results presented here are qualitatively comparable to systems undergoing non-Newtonian flow. We assume that the fluid can be described as a single fluid phase because the concentration fluctuations in the miscible polymer blend are sufficiently small. In the current study we use the lattice Boltzmann method [8] to solve the hydrodynamics of these systems. The flow fields could also be calculated using any Navier-Stokes solver [9,10]; however, the LB method is well suited for incorporating complex boundaries [11–14].

It should be noted that the simulation of porous media using the LB method can result in regions where the flow field is not accurately captured. That is, in regions where the spacing between the solid inclusions is small the flow field is subject to finite-size effects. However, the flow in such regions is small and the majority of the fluid can circumvent these regions if the porosity is high enough. We consider porosity values ranging from 0.5 to 0.85 in the current simulations.

The LB model consists of particle distribution functions which describe, in an averaged sense, mesoscopic fluid "particles" at discrete locations in space traveling with discrete velocities in given directions (i.e., towards nearest and next-nearest neighbors). In other words, while the particle distribution is both discretized in space, velocity, and time, the distribution function itself is continuous.

The LB particle distribution function is evolved using the following equation:

$$f_i(\mathbf{r}+\mathbf{e}_i\Delta t, t+\Delta t) = f_i^{\star}(\mathbf{r},t) = f_i(\mathbf{r},t) + \Omega_i[\mathbf{f}(\mathbf{r},t)], \quad (1)$$

where $f_i(\mathbf{r},t)$ is the density of fluid particles at position $\mathbf{r}$, time t, and with a velocity $\mathbf{e}_i$ [15] and $\mathbf{f}$ is a vectorial representation of the 19 lattice populations, $f_i(\mathbf{r},t)$. The system evolves through both the propagation and subsequent collision of fluid particles. In particular, fluid particles are streamed from each lattice site to neighboring lattice sites, and as the fluid particles reach their destination site they collide. This is illustrated in the above equation through the inclusion of the post-collision term $f_i^{\star}(\mathbf{r},t)$. The collision operator $\Omega_i[\mathbf{f}(\mathbf{r},t)]$ relaxes the stresses toward local equilibrium and, essentially, accounts for instantaneous collisions between fluid particles at the lattice nodes [16].

Given that fluid particles propagate from one lattice site to the next in a given time step, the velocities in the system are discretized. In the simulations presented here the lattice spacings Δx and time step Δt are both assumed to be unity. There are 19 fluid velocities in the three-dimensional model used here (referred to as D3Q19) which correspond to a rest velocity ($\mathbf{e}=[000]$) and velocities in the nearest-($\mathbf{e}=\{100\}$) and next-nearest-neighbor ($\mathbf{e}=\{110\}$) directions.

The velocity moments of the particle distribution function are the hydrodynamic quantities, mass density ρ, momentum density $\mathbf{j}$, and the momentum flux $\boldsymbol{\Pi}$. These are given by

$$\rho = \sum_i f_i,$$

$$\mathbf{j} = \sum_i f_i \mathbf{e}_i = \rho \mathbf{v},$$

$$\Pi = \sum_i f_i \mathbf{e}_i \mathbf{e}_i, \quad (2)$$

where $\mathbf{v}$ is the fluid velocity.

For brevity, we refer the interested reader to the review paper by Chen and Doolen [8] for an overview of the LB method and Refs. [13–18] for a more in-depth description of the model used in this work.

In order to induce flow, an externally applied force term is used to mimic external pressure gradients and the post-collision particle distribution function is modified to read

$$f_i^{\star}(\mathbf{r},t) = f_i(\mathbf{r},t) + \Omega_i[\mathbf{f}(\mathbf{r},t)] + \frac{a_i(\mathbf{e}_i \cdot \mathbf{F}_i)}{c_f^2}, \quad (3)$$

where $\mathbf{F}_i$ are the applied forces [16]. The magnitude of the velocities in the simulation can be varied by changing the magnitude of this term and, in effect, changing the magnitude of the pressure gradient across the system.

The boundaries are included using a nonslip bounce-back scheme [16]. This scheme takes a particle distribution as it streams towards a wall node and bounces it back to the node it came from. For stationary walls, this is described by the propagation step $f_k(\mathbf{r},t+\Delta t)=f_i^{\star}(\mathbf{r},t)$, where k represents the direction opposite to the i direction.

B. Structure factor

The dynamics of a polymer blend can be described using the Cahn-Hilliard-Cook model, which captures the diffusive dynamics of these systems [19–21]. This approach has been extended to include the effects of convective fluid flow in the system [22]. This is done through the addition of a convection term in the following dynamic equation:

$$\frac{\partial \phi}{\partial t} - \mathbf{v} \cdot \boldsymbol{\nabla} \phi = -M \nabla^2 \frac{\partial F}{\partial \phi} + \eta, \quad (4)$$

where ϕ is a conserved order parameter and represents the concentration of one of the polymer components, $\mathbf{v}$ is the fluid velocity, M is the kinetic coefficient, or mobility, F is the free energy of the system, and η is the Cookean noise term [22,23]. This Cookean noise term is Gaussian in nature and accounts for thermal fluctuations. In the absence of the convection term (given by $\mathbf{v}\cdot\boldsymbol{\nabla}\phi$) the model is often used to describe the phase separation dynamics of a binary system and correctly predicts the $t^{1/3}$ Lifshitz-Slyozov domain growth law [24]. Through the inclusion of the convection term, however, this equation has been used to simulate phase separation under shear [22]. It has been found that domains become highly elongated in the flow direction [22,23].

This model can be further extended to describe the dynamics of polymer blends by including the following Flory-Huggins free energy of mixing:

$$\frac{F}{k_\beta T} = \int_V \frac{\phi}{N_A} \ln \phi + \frac{1-\phi}{N_B} \ln(1-\phi) + \chi\phi(1-\phi) + k|\boldsymbol{\nabla}\phi|^2 d\mathbf{r}, \quad (5)$$

where N_A and N_B are the degrees of polymerization for the A and B polymers, respectively, χ is the enthalpic interaction

parameter, and k represents the interfacial tension [25,26]. The first two terms in the above equation describe the entropy of mixing, and the third term describes the enthalpy of mixing, while the final term is from de Gennes [26] and energetically penalizes concentration gradients.

The velocity included in the convection term from the evolution equation is typically considered to be a simple shear flow. However, in this study we consider the convection term to incorporate all flow fields and take the velocity to be of the form

$$\mathbf{v} = \begin{pmatrix} v_{x0} + \frac{\partial v_x}{\partial x}x + \frac{\partial v_x}{\partial y}y + \frac{\partial v_x}{\partial z}z \\ v_{y0} + \frac{\partial v_y}{\partial x}x + \frac{\partial v_y}{\partial y}y + \frac{\partial v_y}{\partial z}z \\ v_{z0} + \frac{\partial v_z}{\partial x}x + \frac{\partial v_z}{\partial y}y + \frac{\partial v_z}{\partial z}z \end{pmatrix}, \tag{6}$$

where v_{x0}, v_{y0}, and v_{z0} are the background velocity fields, which are not relevant to the local variations in composition (note that only gradients in the velocity field will result in the extension or rotation of polymer domains). The remaining terms in the above expression account for the spatial gradients in the velocity field.

In the present study, we are interested in simulating the evolution of the structure factor. This is defined as the Fourier transform of the spatial correlation function of concentration fluctuations. Assuming these fluctuations are small the evolution of the structure factor can be written in the following form:

$$\begin{aligned} \frac{\partial S_{\mathbf{q}}}{\partial t} &- q_x\left[\frac{\partial v_x}{\partial x}\frac{\partial S_{\mathbf{q}}}{\partial q_x} + \frac{\partial v_x}{\partial y}\frac{\partial S_{\mathbf{q}}}{\partial q_y} + \frac{\partial v_x}{\partial z}\frac{\partial S_{\mathbf{q}}}{\partial q_z}\right] \\ &- q_y\left[\frac{\partial v_y}{\partial x}\frac{\partial S_{\mathbf{q}}}{\partial q_x} + \frac{\partial v_y}{\partial y}\frac{\partial S_{\mathbf{q}}}{\partial q_y} + \frac{\partial v_y}{\partial z}\frac{\partial S_{\mathbf{q}}}{\partial q_z}\right] \\ &- q_z\left[\frac{\partial v_z}{\partial x}\frac{\partial S_{\mathbf{q}}}{\partial q_x} + \frac{\partial v_z}{\partial y}\frac{\partial S_{\mathbf{q}}}{\partial q_y} + \frac{\partial v_z}{\partial z}\frac{\partial S_{\mathbf{q}}}{\partial q_z}\right] \\ &= -4Mq^2[\chi_s - \chi + kq^2]S_q + 2Mq^2, \end{aligned} \tag{7}$$

where $\mathbf{q}$ is the scattering vector and χ_s is the χ parameter on the quiescent spinodal, given by

$$2\chi_s = \frac{1}{\phi N_A} + \frac{1}{(1-\phi)N_B}. \tag{8}$$

In the quiescent limit (i.e., when the velocity field reduces to zero) the following equilibrium expression for the structure factor emerges:

$$S_{\mathbf{q}} = \frac{1}{2(\chi_s - \chi + k\mathbf{q}^2)}, \tag{9}$$

which has the correct Ornstein-Zernike form [6].

Lai and Fuller [27] have used this approach to simulate the time evolution of $S_{\mathbf{q}}$ subject to simple shear flow. They found that the structure factor elongates perpendicular to the direction of flow (i.e., the domains in real space elongate in the direction of fluid flow). However, we consider contributions from all spatial gradients in the velocity field. We can, therefore, capture the time evolution of $S_{\mathbf{q}}$ in a system where the velocity fields not only vary with time, but are also nontrivial.

We rewrite the above expression in dimensionless units and, for computational efficiency, consider variations in the structure factor rather than the structure factor directly. In converting the above equations into dimensionless units we follow Lai and Fuller [27]. The dimensionless scattering factor is defined as $\mathbf{k} \equiv \xi\mathbf{q}$, where ξ is the correlation length of the fluctuations. This correlation length is given by $\xi \equiv \sqrt{Mt_R}$ which relates the length and time scales; note that the mobility coefficient is given by $M = \xi^2/t_R$. The dimensionless time is defined as $\tau \equiv t/t_R$ where t_R is the diffusive relaxation time. The interfacial thickness is taken as $\epsilon \equiv \sqrt{k/(2\chi_s - 2\chi)}$, and $L \equiv \epsilon^2/\xi^2$ is the square of the ratio between the interfacial width and the correlation length.

We have found it computationally more efficient to evolve the variations in the structure factor (from the quiescent values) rather than evolve the structure factor directly. The variation in the structure factor, $\Delta S_{\mathbf{k}}$, can be defined as

$$S_{\mathbf{k}} = S_{\mathbf{k}0} + \Delta S_{\mathbf{k}} = \frac{1}{(2\chi_s - 2\chi)(1 + Lk^2)} + \Delta S_{\mathbf{k}}, \tag{10}$$

where $S_{\mathbf{k}0}$ is the quiescent structure factor (in the absence of imposed velocity fields). We can now obtain the following evolution equation:

$$\begin{aligned} \frac{\partial \Delta S_{\mathbf{k}}}{\partial \tau} &= k_x\left[\frac{\partial v_x}{\partial x}\frac{\partial S_{\mathbf{k}0}}{\partial k_x} + \frac{\partial v_x}{\partial y}\frac{\partial S_{\mathbf{k}0}}{\partial k_y} + \frac{\partial v_x}{\partial z}\frac{\partial S_{\mathbf{k}0}}{\partial k_z}\right] \\ &+ k_y\left[\frac{\partial v_y}{\partial x}\frac{\partial S_{\mathbf{k}0}}{\partial k_x} + \frac{\partial v_y}{\partial y}\frac{\partial S_{\mathbf{k}0}}{\partial k_y} + \frac{\partial v_y}{\partial z}\frac{\partial S_{\mathbf{k}0}}{\partial k_z}\right] \\ &+ k_z\left[\frac{\partial v_z}{\partial x}\frac{\partial S_{\mathbf{k}0}}{\partial k_x} + \frac{\partial v_z}{\partial y}\frac{\partial S_{\mathbf{k}0}}{\partial k_y} + \frac{\partial v_z}{\partial z}\frac{\partial S_{\mathbf{k}0}}{\partial k_z}\right] \\ &+ k_x\left[\frac{\partial v_x}{\partial x}\frac{\partial \Delta S_{\mathbf{k}}}{\partial k_x} + \frac{\partial v_x}{\partial y}\frac{\partial \Delta S_{\mathbf{k}}}{\partial k_y} + \frac{\partial v_x}{\partial z}\frac{\partial \Delta S_{\mathbf{k}}}{\partial k_z}\right] \\ &+ k_y\left[\frac{\partial v_y}{\partial x}\frac{\partial \Delta S_{\mathbf{k}}}{\partial k_x} + \frac{\partial v_y}{\partial y}\frac{\partial \Delta S_{\mathbf{k}}}{\partial k_y} + \frac{\partial v_y}{\partial z}\frac{\partial \Delta S_{\mathbf{k}}}{\partial k_z}\right] \\ &+ k_z\left[\frac{\partial v_z}{\partial x}\frac{\partial \Delta S_{\mathbf{k}}}{\partial k_x} + \frac{\partial v_z}{\partial y}\frac{\partial \Delta S_{\mathbf{k}}}{\partial k_y} + \frac{\partial v_z}{\partial z}\frac{\partial \Delta S_{\mathbf{k}}}{\partial k_z}\right] \\ &- 4(\chi_s - \chi)\mathbf{k}^2(1 + L\mathbf{k}^2)\Delta S_{\mathbf{k}}, \end{aligned} \tag{11}$$

where the derivatives of the velocity field are dimensionless (with respect to the relaxation time) and are allowed to vary as a function of time during the simulation. We can, therefore, simulate the evolution of the structure factor for a given element of fluid subject to complex time-dependent spatial velocity derivatives.

C. Multiscale model

We consider the dynamics of fluid flow through porous media and, given the complex flow patterns, predict the evolution of the concentration fluctuations. The history of a fluid element as it travels through the porous media influences the

structure factor associated with that fluid element. In other words, in order to obtain the structure factor at a given point in space we have to consider the pathway traversed by the fluid element to reach that point. To do this we construct a streamline following the path of a fluid element as it travels through the porous media up to the point where we wish to calculate the structure factor. By considering the velocity gradients experienced by the fluid element as a function of time as it traverses the system we can now evolve the structure factor calculation [Eq. (11)]. We calculate the structure factor as a function of time for this fluid element and take into consideration the variations in velocity gradients it experiences along its journey through the porous media.

We simulate the flow through porous media by first creating the tortuous pathways for fluid flow through the system. The LB lattice is $400\times 50\times 50\Delta x^3$ in size, and periodic boundary conditions are applied in all directions. This approach has the benefit of reducing finite-size effects. The porous media are constructed by randomly placing immovable spherical regions of radius $10\Delta x$ (allowing spheres to overlap) until the relative volume of free space, or porosity, reaches a desired value. The fluid is then forced to move in the x direction through the application of an external force, which mimics the application of a pressure gradient. We evolve the system until the variation in velocities reaches zero and the flow has reached steady state.

In this study we are not only interested in the flow profiles, but also wish to follow fluid elements as they travel through the system and investigate the effects of spatial variations in velocity on the polymer blend concentration fluctuations. To do this we monitor the progress of a fluid element and evolve its position as a function of the local velocity multiplied by a small time step. In particular, we linearly interpolate the velocity of the fluid in between lattice sites and also the spatial derivatives of the velocity (which are necessary for evolving the structure factor). We can now follow a fluid element as it flows through the system. In particular, we can use the position and velocity of a fluid element to evolve its position given an increment in time and obtain a new position. In this manner, we follow the fluid element as it traverses the porous media and output the spatial derivatives experienced by the fluid element as a function of time. Therefore, we can obtain the local spatial gradients of the velocity that act on a fluid particle as a function of time as it travels through the complex and tortuous system. The spatial derivatives of the velocity as a function of time now serves as the input to the Cahn-Hilliard model. The structure factor of the concentration fluctuations is allowed to evolve subject to these extensional and shear flows. In particular, variations in velocity fields are key to describing the evolution of the polymer blend and we incorporate these derivatives from the LB model into Eq. (16) above. Therefore, we can simulate the elongation and rotation of concentration fluctuations in the polymer blend as a consequence of the complex flow patterns experienced while flowing through porous media. We now demonstrate this multiscale approach and present results which correlate the tortuosity of a fluid channel with the concentration fluctuations of a polymer blend flowing through this channel.

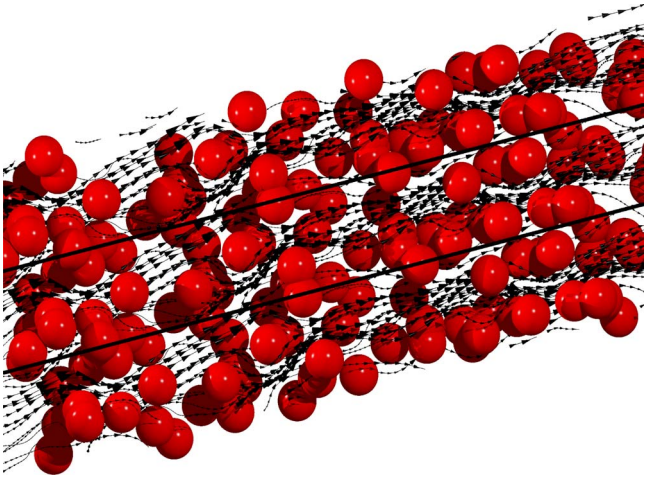

FIG. 1. (Color online) The flow field through a system of 80% porosity. The red spheres represent solid regions, and the black lines are streamlines through the system. Cones represent the velocity of the fluid with orientation and size corresponding to the direction and magnitude of the fluid flow.

III. RESULTS AND DISCUSSION

In this section we present results of fluid flow in porous media. We then demonstrate how these flow fields can have a dramatic impact on the evolution of the structure factor of the polymer blend concentration fluctuations.

The flow field through a system containing a porosity of 0.8 is shown in Fig. 1. The solid spheres are placed at random (and allowed to overlap) in the LB lattice until the amount of space taken up by the particles reaches 20%. The remaining 80% of the system is fluid (hence, a porosity of 0.8). The solid spheres are depicted and the fluid flow is illustrated by "streamlines," pathways along which the fluid flows through the system. Cones, whose orientation and size depict the direction and magnitude of the velocity field, are included along these streamlines. For clarity, we show three realizations of the computational domain, side by side, reflecting the periodicity of the simulations.

The random placements of solid spheres in the channel results in the fluid having to flow around these obstructions and the streamlines are, therefore, tortuous. That is, the path which the fluid travels is increased in distance as it has to snake its way through the complex and convoluted system. Another feature of the flow profile is the convergence of fluid into regions in between solid spheres and the relatively high velocity fields in these regions.

In Fig. 2 we quantify the tortuosity of systems with porosity ranging from 0.85 to 0.5 (we simulate three different configurations for each porosity). The tortuosity is defined as being the ratio between the length of the flow path of a fluid element through the sample and the length of the system [7]. We take the tortuosity of paths which begin at one end of the system and travel through to the other end of the system. Pathways which are completely obstructed by the solid spheres (i.e., the fluid streamline flows directly into a sphere or cluster of spheres such that the velocity goes to zero) are not considered. Figure 2 depicts the cumulative distribution

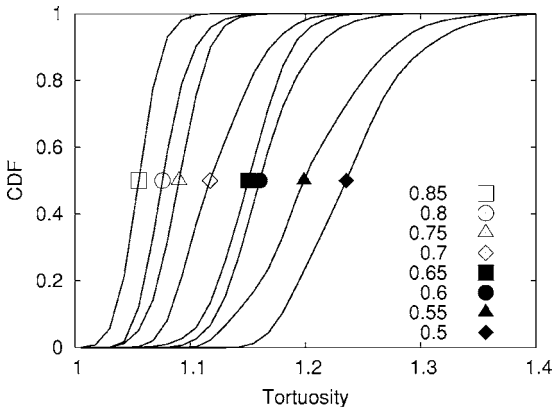

FIG. 2. Cumulative distribution function (CDF) of the tortuosity of systems with varying porosity (ranging from 0.5 to 0.85).

function (CDF [28]) of the tortuosity for systems with different porosity (and three independent runs for each porosity value). As the porosity is reduced and more obstacles are placed in the fluids path, the average tortuosity of the systems increases. The average tortuosity increases from roughly 1.05 to 1.23, as the porosity is reduced from 0.85 to 0.5.

During these simulations the same internal body force was maintained, which is equivalent to applying a constant global pressure difference across the systems. Therefore, as the number of solid spheres is increased (and the porosity decreases) the overall velocity in the system is reduced. This is illustrated in Fig. 3 which depicts the CDF of the local velocity magnitude in systems of varying porosity. Again, we consider three independent runs for each porosity value. Not only is the average value of the velocities significantly reduced on increasing the number of solid spheres (and, hence, increasing the area of no flux surfaces in the system), but the width of the distributions would also appear to be narrower.

The flow field influences the structure factor of the concentration fluctuations through spatial velocity derivatives. We plot the derivatives of the velocity in the flow direction with respect to perpendicular directions [$\delta_y v_x$ and $\delta_z v_x$ in Fig. 4(a)] and the flow direction [$\delta_x v_x$ in Fig. 4(b)]. In other

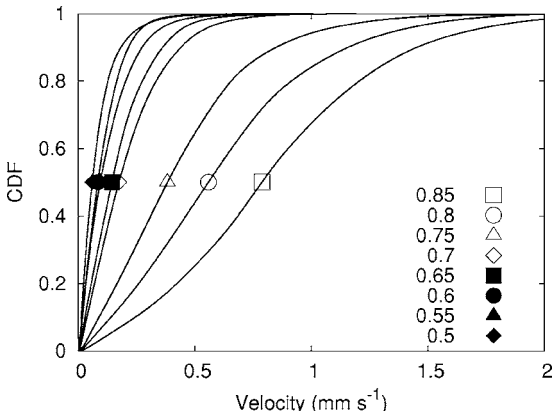

FIG. 3. Cumulative distribution function (CDF) of the local velocity magnitude in systems with varying porosity (ranging from 0.5 to 0.85).

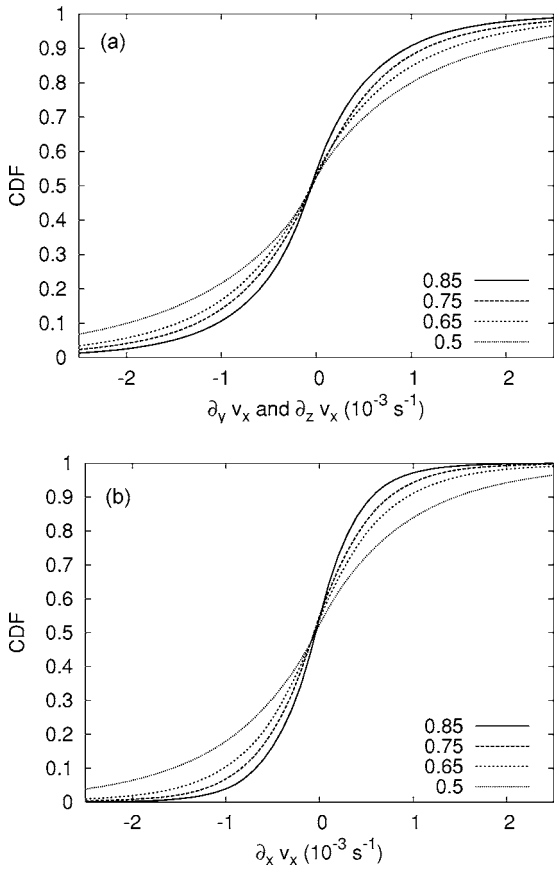

FIG. 4. Cumulative distribution function (CDF) of the local velocity gradients (a) $\delta_y v_x$ and $\delta_z v_x$, and (b) $\delta_x v_x$, in systems with varying porosity (ranging from 0.5 to 0.85).

words, we isolate the shear and extensional components of the velocity gradients in the flow direction (it should be noted that the remaining spatial derivatives exhibit similar trends). We normalize the local velocity in a system (and, hence, the velocity derivatives) by the average velocity in that system and, thereby, isolate the effects of tortuosity on the spatial gradients. In effect, all fluid elements travel on average at the same speed, but the more tortuous paths take longer as they travel farther. The CDF's of the normalized velocity gradients are obtained from three independent runs for each porosity. We find that the average velocity gradients are around zero and the distribution extends farther for systems with lower porosity. Therefore, the more complex and tortuous the flow fields, the larger the spatial derivatives of the velocity fields. We now seek to correlate these derivatives with the evolution of the structure factor of a fluid element as it traverses the porous media and is subject to these derivatives.

Figure 5(a) depicts a streamline through a system with 50% porosity. We isolate a single streamline through the system and depict the solid regions as semitransparent spheres. The magnitude of the spatial derivatives of the velocity field (taken as $\delta_i v_j : \delta_i v_j$) is plotted as a function of time in Fig. 5(b). Positions 1–4 marked in Fig. 5(a) are also shown in Fig. 5(b). As the fluid traverses a tortuous pathway through the system the fluid element travels at different speeds in different regions and experiences different velocity gradients.

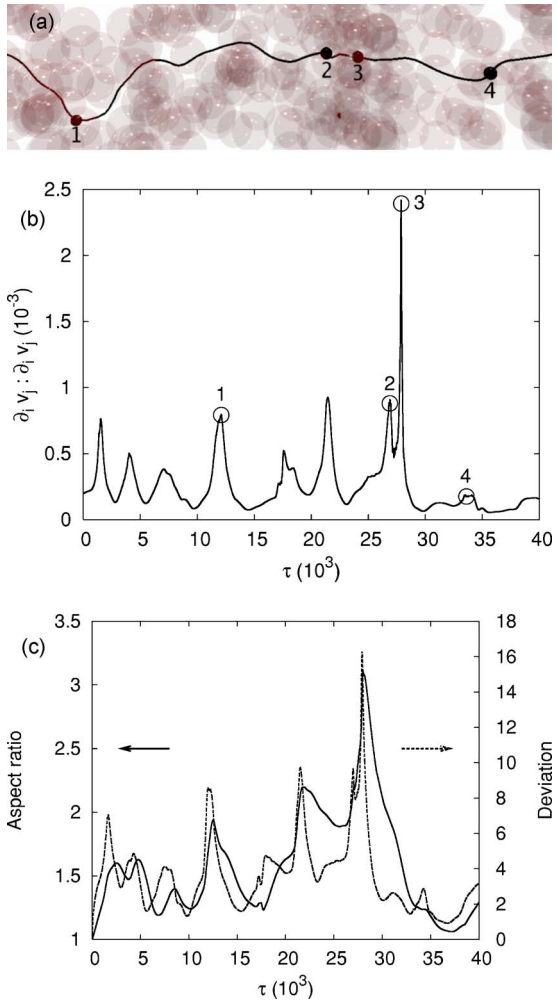

FIG. 5. (Color online) Correlation of pathway, velocity derivatives, and structure factor variations. Shown are (a) streamline through system with 50% porosity (solid regions near to the streamline are shown as semitransparent spheres), (b) the magnitude of the velocity gradients ($\delta_i v_j : \delta_i v_j$) as a function of time, and (c) both the average deviation in $S_{\mathbf{k}}$ and aspect ratio as a function of time. Circles in plot (b) correspond to the numbered position in plot (a).

Areas of twists and turns in the fluid path correspond with sudden increases in velocity gradients. Furthermore, sudden increases in velocity gradients are observed when the fluid is corralled through a narrow region [positions 2 and 3 in Fig. 5(a), for example]. As the fluid is contracted in this region the fluid element experiences significant extensional flows. These velocity gradients can now be correlated with their effects on the structure factor of the concentration fluctuations. As the fluid travels through the porous media we calculate the average deviation of the structure factor from the quiescent structure factor [$\Delta S_{\mathbf{k}}$ averaged over k; see Eq. (15)] and the aspect ratio of the structure factor. The aspect ratio is obtained by considering an isosurface around the structure factor at a value of 75% of the maximum $S_{\mathbf{k}}$ value. We then determine the points on this isosurface which are closest and farthest (in $\mathbf{k}$ space) from the center. The aspect ratio is simply defined as the ratio between the farthest distance and the closest distance. The average deviation of the structure factor from its quiescent state and the aspect ratio are both plotted in Fig. 5(c). These plots should be compared with the plot of $\delta_i v_j : \delta_i v_j$ in Fig. 5(b). The deviation of the structure factor shows a very close correlation to the magnitude of the velocity derivatives. The positions and magnitude of the peaks in both plots appear to be very similar. The aspect ratio, on the other hand, appears to be less correlated with the magnitude of the velocity derivatives. In particular, the aspect ratio exhibits a smoother curve and the peaks are shifted to later times. In other words, there is a response time, or delay, between the fluid element experiencing variations in the velocity derivatives and the structure factor becoming deformed, or elongated.

To further illustrate the effects of the flow field on the structure factor we plot the structure factor [at the various labeled points from Fig. 5(a)] in Fig. 6. The structure factor is three dimensional and, therefore, for clarity we only present half of the system. Isosurfaces are depicted at values of 25% (outer shell), 50% (middle shell), and 75% (inner shell) of the maximum value of the structure factor. In Fig. 6(a) [point No. 1 along the streamline in Fig. 5(a)] the outer contour surface appears to be relatively undeformed, while the inner surfaces would appear to be slightly elongated perpendicular to the flow direction (k_x). Figures 6(b) and 6(c) show the fluid as it is contracted and extended flowing through the narrow channel shown as points 2 and 3 in Fig. 5(a). The surfaces become even more deformed, especially the isosurface at 75% of the maximum $S_{\mathbf{q}}$ value which becomes considerably elongated in the k_y and k_z directions and appears to be tilted. This means that the concentration fluctuations in real space are elongated in the flow direction. As the fluid emerges from the cluster of solid spheres, which contracted and elongated the spatial concentration fluctuations, the velocity gradients subside considerably. At this point [shown in Fig. 6(d)] the structure factor returns towards its quiescent state and the isosurfaces appear to be more spherical.

In order to quantify the correlation between the magnitude of the velocity derivatives [see Fig. 5(b)] and both the deviation of the structure factor and the aspect ratio [see Fig. 5(c)] we calculate correlation functions. The correlation function between two discrete data sets x_i and y_i (which in our case represent velocity derivatives and either the aspect ratio or average deviation of the structure factor) can be written in the form

$$C = \frac{\frac{1}{n-L}\sum_{i=1}^{n-L}(x_i-\mu_x)(y_{i+L}-\mu_y)}{\sigma_x\sigma_y}, \tag{12}$$

where μ_x and σ_x are the average and standard deviation of a discrete time series x_i. Here n represents the total number of discrete values of both x_i and y_i, and L is included to account for a discrete time delay. If the two sets x_i and y_i are perfectly correlated, then the correlation function would return a value of 1. Uncorrelated data sets would return a value of zero, while negatively correlated data [i.e., $x_i-\mu_x \propto -(y_i-\mu_i)$] would return a value of -1. We shift one of our data sets by a discrete amount (represented by the discrete quantity L)

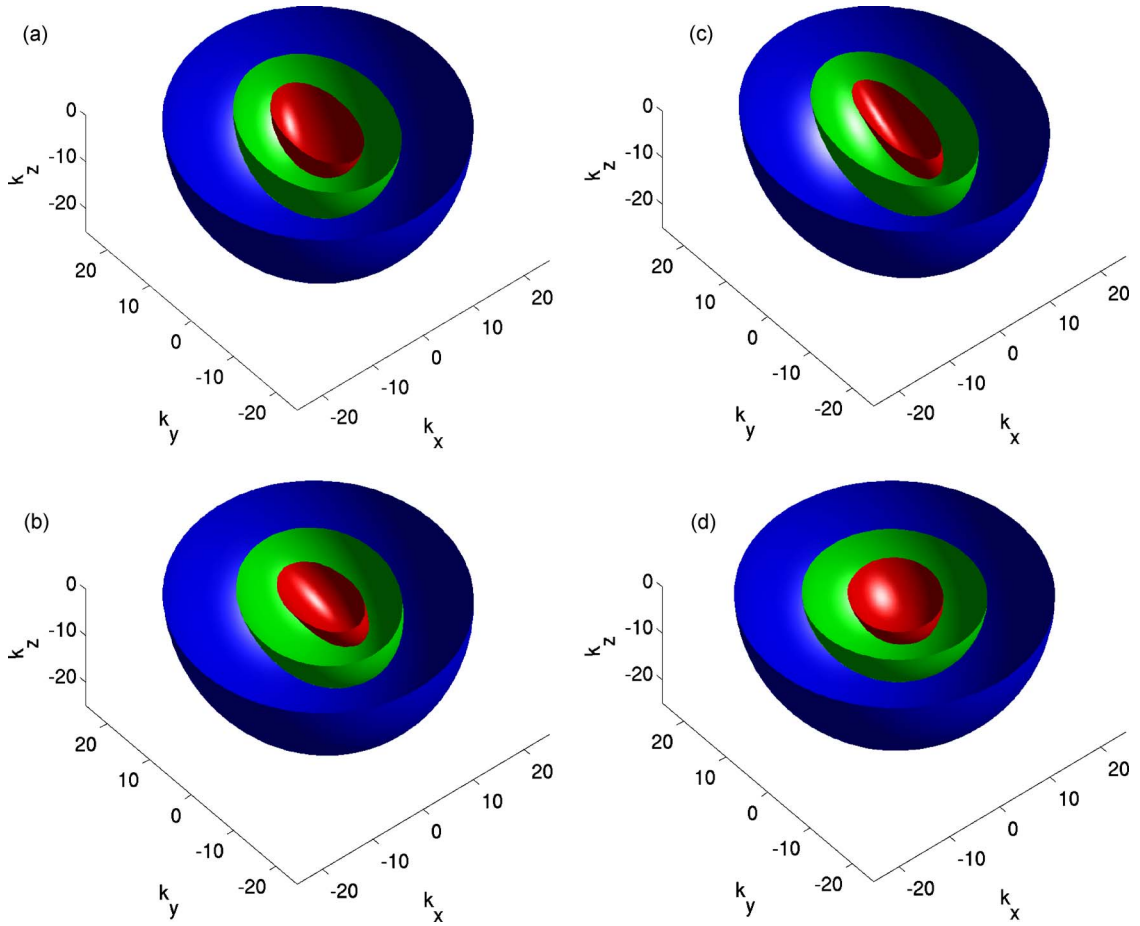

FIG. 6. (Color online) Isosurfaces of the structure factor at the positions numbered from 1 to 4 in Fig. 5(a); in particular, the structure factors at (a) position 1, (b) position 2, (c) position 3, and (d) position 4 are shown. Isosurfaces are depicted at values of 25% (outer shell), 50% (middle shell), and 75% (inner shell) of the maximum value of the structure factor.

and obtain the correlation function as a function of this shift in Fig. 7. We show the correlation functions between the magnitude of the velocity gradients and both the aspect ratio and deviation of the structure factor for the same system (and streamline) as depicted in Fig. 5. The aspect ratio is the least correlated, exhibiting a maximum correlation function of roughly 0.6, and this occurs after a delay of roughly $2\Delta\tau$. On the other hand, the average deviation is much more closely correlated with the magnitude of the velocity derivatives and exhibits a maximum correlation function of roughly 0.9 after a much smaller time. Therefore, in this system, the deviation of the structure factor responds much quicker than the aspect ratio to variations in the magnitude of the velocity gradients and the correlation is more pronounced.

We now quantify this correlation for a number of systems and plot the cumulative distribution functions of the correlation functions for both the average $\Delta S_{\mathbf{k}}$ and the aspect ratio in Fig. 8 (the correlation function is taken to be the maximum correlation function from plots similar to Fig. 7). The correlations are performed on streamlines from systems of various porosity (from 0.5 to 0.85) and over three randomly chosen streamlines (from independent LB simulations) for each value of porosity. The correlation functions between the aspect ratio and the velocity gradients appear to be lower than the correlation functions between the average $\Delta S_{\mathbf{k}}$ and the velocity gradients. The correlation functions are all positive which indicates that there is a definite correlation between the aspect ratio of the structure factor and the magnitude of the velocity gradients. All of the correlation functions between the average $\Delta S_{\mathbf{k}}$ and the velocity gradients, however, are above 0.8 which represents a more significant correlation.

We also consider the response time from the correlation function (defined as the time taken for the correlation function to reach a maximum value in plots similar to Fig. 7). Cumulative distribution functions for the response time associated with the correlation functions between velocity gradients and both the average $\Delta S_{\mathbf{k}}$ and the aspect ratio are plotted in Fig. 9. Not only is the deviation of the structure factor from its quiescent state well correlated with the velocity gradients, but there is also only a small delay between the fluid experiencing the velocity gradients and variations in the structure factor occurring. The aspect ratio, on the other hand, is not as well correlated and experiences a considerable delay between velocity gradients and elongation of the structure factor.

When calculating the aspect ratio of the structure factor (or, rather, the aspect ratio of the isosurface of the structure factor at 75% its maximum value) we also calculate the direction of this elongation. A histogram depicting the average

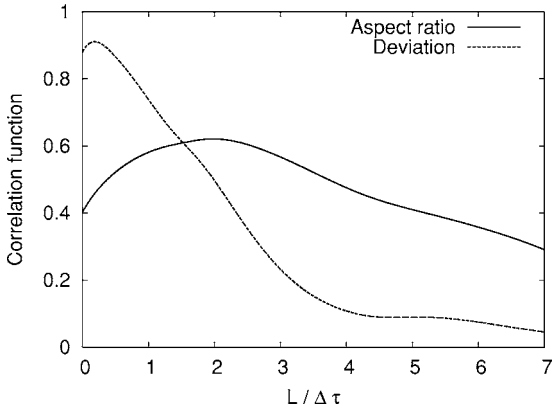

FIG. 7. Correlation functions between the magnitude of the velocity derivatives from the macroscopic fluid dynamics and both the aspect ratio and deviation of the structure factor of the nanoscale concentration fluctuations. The correlation function is plotted as a function of a shift in one of the data sets (see text). The maximum correlation function is taken to be the correlation function between the two sets, and the value of L to obtain this maximum value is taken to be the response time.

angle between this elongation and the flow direction is depicted in Fig. 10. In particular, we weight the contributions from the different angles with respect to the aspect ratio minus one. That is, if the aspect ratio is 1, then the angle of the orientation is not important. However, if the aspect ratio is significantly greater than 1, then the contribution of the angle to the histogram should reflect this. An angle of zero would indicate that the structure factor is elongated in q_x and, therefore, the spatial fluctuations are compressed in the x direction. The statistics indicate that this is unlikely to occur in these systems. More probable is the angle between the elongation and the flow direction being closer to 90°. The structure factor is, therefore, more likely to be compressed into a disk shape which lies in the k_y-k_z plane or elongated in either the k_y or k_z direction. This means that the spatial concentration fluctuations are elongated more towards the flow direction. This is similar to what has been observed in fluid subject to simple shear flow, where the concentration

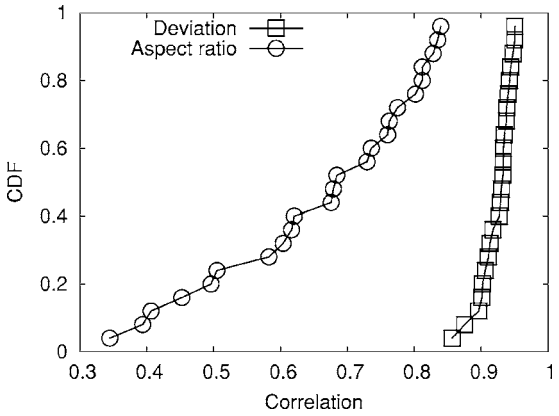

FIG. 8. Cumulative distribution function (CDF) of the correlation function of deviations in $S_{\mathbf{k}}$ and aspect ratio with the magnitude of the velocity gradients.

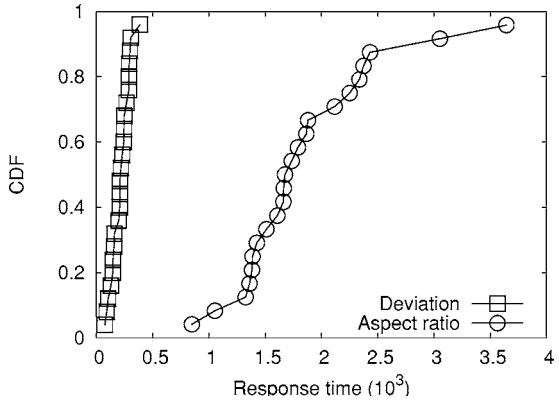

FIG. 9. Cumulative distribution function (CDF) of the response time obtained from the correlation function of deviations in $S_{\mathbf{k}}$ and aspect ratio with the magnitude of the velocity gradients.

fluctuations are also found to elongate towards the flow direction [22]. In particular, in shear flow the elongation occurs at an angle which depends on the strength and duration of the imposed shear flow. Here, however, the flow profile is much more complex and time dependent and we observe concentration fluctuations elongating either in the flow direction or at an acute angle with the flow direction.

IV. SUMMARY AND CONCLUSIONS

We have presented a multiscale approach for simulating a miscible polymer blend flowing through porous media. This approach links the macroscopic flow field with the microscopic concentration fluctuations in polymer blends. In particular, we can follow a specific fluid element as it travels through the porous media and predict the concentration fluctuations in this *exact* fluid element. We find a close correlation between the tortuous pathways, the velocity gradients in the fluid, and the deviations of the structure factor from its

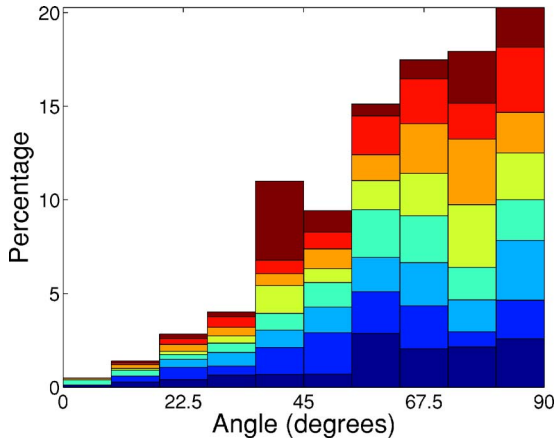

FIG. 10. (Color online) Histogram of the angle between the location of the farthest point on an isosurface (75% of the maximum value) of the structure factor and the flow direction. The contributions are weighted according to the aspect ratio minus 1. Systems with porosity ranging from 0.85 (lowest stacked boxes) to 0.5 (highest stacked boxes) are considered.

quiescent state. The complex flow through porous media appears to elongate the spatial domains in the flow direction (or at an acute angle with the flow direction) rather than in directions perpendicular to the flow direction.

The current investigation has concentrated on miscible polymer blends; however, immiscible polymer blends are more common. While phase separation in complex geometries has been simulated, this is usually on the length scale of the macroscopic geometry. Furthermore, phase-separating blends subject to shear have been the subject of many investigations. However, very little work has been conducted on the effects of more complex flow fields. Future work, therefore, will seek to couple the macroscopic flow fields in porous media with the domain elongation and rotation in phase-separating polymer blends on the microscale.

The analysis of concentration fluctuations in miscible polymer blends offers a unique opportunity to probe the thermodynamics of polymer blend systems. The elongation of the structure factor observed in the current study is similar in many ways to the deformations observed under simple shear flow. Therefore, a phenomenon similar to shear-induced mixing is likely to occur in polymer blends flowing in porous media. Through the simulations presented here we have shown that polymer concentration fluctuations (and, hence, thermodynamic properties such as the interaction parameter) can be related to macroscopic flow fields. In other words, by simply measuring the flow fields in a given system one can draw significant conclusions about the thermodynamics of the system. Vice versa, measurements of the concentration fluctuations in a blend of known thermodynamics can reveal insights into the tortuosity of the flow field. It is expected that the insights gained from this work, into the effects of complex flow on the concentration fluctuations in polymer blends, will stimulate commensurate experimental studies.

[1] D. R. Paul and C. B. Bucknall, *Polymer Blends* (Wiley, New York, 2000).

[2] L. H. Sperling, *Polymeric Multicomponent Materials* (Wiley-Interscience, New York, 1997).

[3] A. Silberberg and W. Kuhn, Nature (London) **170**, 450 (1952).

[4] K. A. Mazich and S. H. Carr, J. Appl. Phys. **54**, 5511 (1983).

[5] N. Clarke, in *Phase Behavior of Polymer Blends*, edited by K. Freed (Springer, New York, 2005), Vol. 183, p. 127.

[6] M. Doi, *Introduction to Polymer Physics* (Clarendon Press, Oxford, 1996).

[7] F. A. L. Dullien, *Porous Media: Fluid Transport and Pore Structure* (Academic Press, Oxford, 1979).

[8] S. Chen and G. D. Doolen, Annu. Rev. Fluid Mech. **30**, 329 (1998).

[9] J. S. Andrade, Jr., M. P. Almeida, J. Mendes Filho, S. Havlin, B. Suki, and H. E. Stanley, Phys. Rev. Lett. **79**, 3901 (1997).

[10] C. Manwart, U. Aaltosalmi, A. Koponen, R. Hilfer, and J. Timonen, Phys. Rev. E **66**, 016702 (2002).

[11] A. Cancelliere, C. Chang, E. Foti, D. H. Rothman, and S. Succi, Phys. Fluids A **2**, 2085 (1990).

[12] M. Kraczak, M. Cerrolaza, M. Schulz, and E. Rank, J. Biomech. **31**, 453 (1993).

[13] R. Verberg and A. J. C. Ladd, Phys. Rev. E **65**, 056311 (2002).

[14] G. A. Buxton, R. Verberg, D. Jasnow, and A. C. Balazs, Phys. Rev. E **71**, 056707 (2005).

[15] U. Frisch, D. d'Humieres, B. Hasslacher, P. Lallemand, Y. Pomeau, and J.-P. Rivet, Complex Syst. **1**, 649 (1987).

[16] A. J. C. Ladd and R. Verberg, J. Stat. Phys. **104**, 1191 (2001) and references therein.

[17] X. He and L.-S. Luo, Phys. Rev. E **55**, R6333 (1997); **56**, 6811 (1997).

[18] D. d'Humieres, I. Ginzburg, M. Krafczyk, P. Lallemand, and L.-S. Luo, Philos. Trans. R. Soc. London, Ser. A **360**, 437 (2002).

[19] J. W. Cahn and J. E. Hilliard, J. Chem. Phys. **28**, 258 (1958).

[20] J. W. Cahn, J. Chem. Phys. **42**, 93 (1965).

[21] S. C. Glotzer, Annu. Rev. Comput. Phys. **2**, 1 (1995).

[22] T. Ohta, H. Nozaki, and M. Doi, J. Chem. Phys. **93**, 2664 (1990).

[23] G. A. Buxton and A. C. Balazs, Phys. Rev. B **69**, 054101 (2004).

[24] I. M. Lifshitz and V. V. Slyozov, J. Phys. Chem. Solids **19**, 35 (1961).

[25] P. J. Flory, *Principles of Polymer Chemistry* (Cornell University press, Ithaca, 1953).

[26] P. G. de gennes, J. Chem. Phys. **72**, 4756 (1980).

[27] J. Lai and G. G. Fuller, J. Polym. Sci., Part B: Polym. Phys. **32**, 2461 (1994).

[28] The CDF completely describes the distribution of a variable and is defined as the integration of the probability distribution function. Mathematically, this is written as CDF $(x) = \int_{x\,min}^{x} p(\hat{x}) d\hat{x}$, where $p(x)$ is the probability distribution function. Therefore, the CDF varies from 0 to 1 as the sum of all probabilities is equal to 1.